ChemComm

Design of V-shaped ionic liquid crystals: Atropisomerisation ability and formation of double-gyroid molecular assemblies

Journal:	*ChemComm*
Manuscript ID	CC-COM-06-2024-003002.R3
Article Type:	Communication

ChemComm

COMMUNICATION

Design of V-shaped ionic liquid crystals: Atropisomerisation ability and formation of double-gyroid molecular assemblies

Received 00th January 20xx,
Accepted 00th January 20xx

DOI: 10.1039/x0xx00000x

Takahiro Ichikawa,*[a] Soki Obara,[a] Saori Yamaguchi,[a] Yumin Tang,[b] Toshiyo Kato,[c] and Xiangbing Zeng[b]

We designed V-shaped ionic liquid crystals with two sterically congested ionic parts at the vertex. Depending on the degree of steric hindrance, atropisomerisation occurred in solution. All compounds formed bicontinuous cubic phases with double-gyroid structures in the bulk state, partially owing to the co-existence of atropisomers with opposite chirality.

Bicontinuous cubic (Cub_{bi}) phase is a nanosegregated liquid-crystalline (LC) phase in which two incompatible molecular parts form 3D continuous domains.[1] Cub_{bi} phases appear between lamellar and columnar phases in lyotropic[2] and thermotropic[3] liquid crystals. The volume balance between the incompatible parts is a critical parameter for creating liquid crystals that form Cub_{bi} LC assemblies. For lyotropic liquid crystals, the volume balance can be tuned continuously by adjusting the solvent weight percentage, which facilitates the design of lyotropic Cub_{bi} LC assembles. In contrast, the design of thermotropic Cub_{bi} LC assembles is challenging because slight changes in the molecular structure of thermotropic liquid crystals influence both the polar/non-polar volume balance and the strength of intermolecular interactions.[3,4]

Owing to their unique nanostructure, Cub_{bi} liquid crystals are attractive as transport materials[5] and separation membranes.[6] To further accelerate research on the applications of Cub_{bi} liquid crystals, new design principles must be developed and evaluated. Recent reports have revealed that in addition to the chemical structure, the conformational structure, especially in the bulk state, is involved in the formation of Cub_{bi} LC assemblies.[7,8] For example, Tschierske et al. showed that a series of polycatenar rod-like molecules with a 5,5′-diphenylbithiophene core form right- or left-handed chiral assemblies in local domains owing to chirality synchronisation of the close-packed molecules, which leads to the formation of triple network Cub_{bi} LC assemblies.[7a,b] Yamamoto et al. reported that the racemic mixture of a dichiral rod shape compound form a cubic phase while the increase of the optical purity of the racemic mixture leads to the exhibition of smectic Q phases.[7c] These pioneering examples lead us to expect that, equal amounts of two conformers with opposite chiralities could plausibly contribute to the formation of gyroid-Cub_{bi} phases because they have a double-gyroid structure, in which two single gyroids with opposite chiralities are interwoven. We previously reported that V-shaped ionic compounds **[Me-Im][X]** (n = 12 and 14) (Fig. 1a) with a dicyanobenzene core and two methylimidazolium cations at the vertex undergo atropisomerisation in solution and form thermotropic gyroid-Cub_{bi} LC phases in the bulk state.[8] Although it remains unclear whether atropisomerisation leads directly to the formation of gyroid-Cub_{bi} LC molecular assemblies, these observations suggest a new design principle for thermotropic gyroid-Cub_{bi} liquid crystals. Therefore, we were inspired to investigate the atropisomerisation ability and thermotropic LC behaviour of **[Me-Im][X]** analogues.

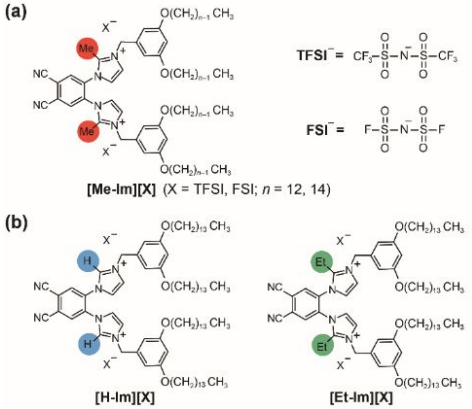

Fig. 1. Molecular structures of (a) **[Me-Im][X]** (n = 12 and 14) designed in our previous study[8] and (b) **[H-Im][X]** and **[Et-Im][X]** designed in the present study.

[a] *Department of Biotechnology and Life Science, Tokyo University of Agriculture and Technology, Tokyo 184-8588, Japan*
E-mail: t-ichi@cc.tuat.ac.jp
[b] *Department of Materials Science and Engineering, University of Sheffield, Sheffield S1 3JD, UK*
[c] *Smart-Core-Facility Promotion Organization, Tokyo University of Agriculture and Technology, Tokyo 184-8588, Japan*
Electronic Supplementary Information (ESI) available. See DOI: 10.1039/x0xx00000x

In this study, we designed V-shaped ionic compounds **[H-Im][X]** and **[Et-Im][X]** (Fig. 1b) with four tetradecyl alkyl chains. These compounds are analogous to **[Me-Im][X]** (n = 14), with the only difference being that the methyl group at the 2-position of each imidazolium ring is replaced by a proton in **[H-Im][X]** and an ethyl group in **[Et-Im][X]**. We examined the effects of bulkiness at the 2-position of the imidazolium rings on the rotation barrier of the C–N bonds between the dicyanobenzene moiety and the imidazolium rings. Furthermore, we investigated the relationship between atropisomerisation ability in solution and molecular-assembly behaviour in the bulk state.

The atropisomerisation abilities of **[H-Im][TFSI]** and **[Et-Im][TFSI]** were investigated using ^{1}H-NMR measurements in acetone-d_6 and DMSO-d_6, respectively. For **[Et-Im][TFSI]**, the signals corresponding to the protons on the imidazolium rings appear as broad peaks at 7.5–8.0 ppm at room temperature (Fig. 2a). These peaks become broader upon increasing the temperature to 50 °C but then sharpen at higher temperatures. This behaviour, which is similar to that previously observed for **[Me-Im][TFSI]**,[8] can be explained by the formation of three conformers, denoted as *R*, *S*, and *meso* (Fig. S26). Thus, the C–N bond between dicyanobenzene and the imidazolium ring (C_{Bz}–N_{Im} bond) has a moderate rotation barrier. In contrast, the proton signals of the imidazolium rings of **[H-Im][TFSI]** appear as sharp peaks at room temperature (Fig. 2b). This sharpness is maintained at lower temperatures, such as 0 °C, indicating that C_{Bz}–N_{Im} bond rotation in **[H-Im][TFSI]** is feasible in solution. A similar trend was observed for the corresponding compounds with FSI anions (see the ESI). Based on these results, we conclude that the rotational barriers of the two C_{Bz}–N_{Im} bonds in these compounds strongly depend on the bulkiness of the substituent at the 2-position of the imidazolium ring.

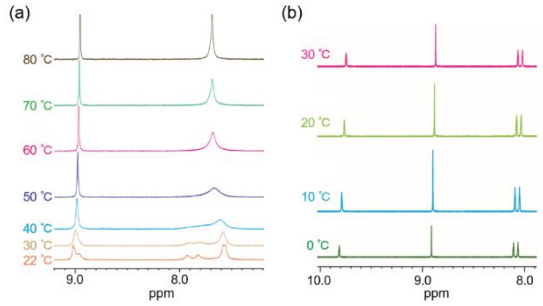

Fig. 2. ^{1}H-NMR spectra of (a) **[Et-Im][TFSI]** in DMSO-d_6 at temperatures of 22–80 °C and (b) **[H-Im][TFSI]** in acetone-d_6 at temperatures of 0–30 °C.

The peaks in the ^{1}H-NMR spectra of the compounds were assigned using ^{1}H NOESY NMR, a 2D NMR method that reveals through-space correlations via spin–lattice relaxation. The ^{1}H NOESY NMR profile of **[Et-Im][TFSI]** in DMSO-d_6 at 25 °C is shown in Fig. 3a. To simplify the discussion, specific protons in half of the **[Et-Im][TFSI]** molecule were named ***a*–*e***, and the corresponding protons in the other half were named ***a*′–*e*′** (Fig. 3b). The signals at 5.38, 6.30, and 6.45 ppm were assigned to ***a*–*c*** based on general insights[9] and previous results (Fig. 3c).[8] Although the three peaks at 7.5–8.0 ppm correspond to ***d*** and ***e***, these signals could not be assigned using general insights alone. Therefore, we focused on the correlations between ***a*–*c*** and the three peaks at 7.5–8.0 ppm. Proton ***a*** exhibits significant correlations with the signals at 7.57 and 7.82 ppm but a negligible correlation with that at 7.92 ppm. A similar trend is observed for ***b***, whereas no correlations appear between ***c*** and these three peaks. Thus, the correlation between the signal at 7.57 ppm and ***a*(*b*)** is attributed to the proximity of ***e***′ and ***a*(*b*)** in the *R*/*S* conformers. Furthermore, the corelation between the signal at 7.82 ppm and ***a*(*b*)** is attributed to the proximity of ***d***′ and ***a*(*b*)** in the *R*/*S* conformers. In contrast, the negligible correlation between the signal at 7.92 ppm and ***a*(*b*)** can be explained by assigning this peak to ***d*** in the *meso* conformers, in which ***d*** is far away from ***a***′, ***b***′, and ***c***′ in the other half of the molecule. Based on these results, the signal at 7.57 ppm corresponds to ***e*** in both the *R*/*S* and *meso* conformers, whereas the signals at 7.82 and 7.92 ppm correspond to ***d*** in the *R*/*S* and *meso* conformers, respectively. This assignment is supported by the fact that the sum of the areas of the peaks at 7.82 and 7.92 ppm is nearly equal to the area of the peak at 7.57 ppm.

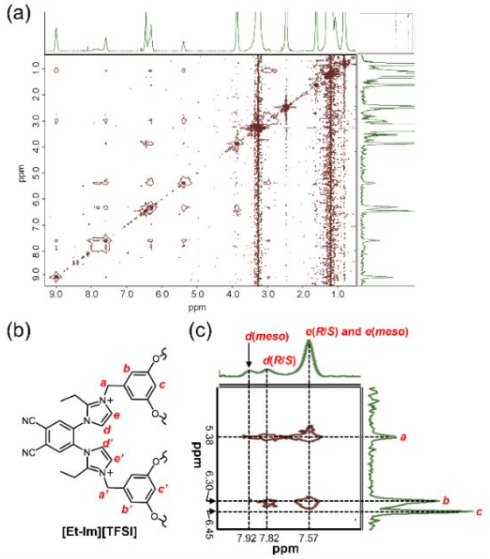

Fig. 3. (a) ^{1}H NOESY NMR profile of **[Et-Im][TFSI]** in DMSO-d_6 (500 MHz, 25 °C). (b) Molecular structure of **[Et-Im][TFSI]** and assignment of protons ***a*–*e*** and ***a*′–*e*′**. (c) Enlargement of the ^{1}H NOESY NMR profile.

To estimate the energy barrier for rotation around the C_{Bz}–N_{Im} bond ($\Delta G^{\ddagger}$), we analysed the temperature dependence of the peak areas and positions of ***d*(*meso*)** and ***d*(*R*/*S*)**. Based on the ^{1}H NMR results and the Eyring equation,[10] $\Delta G^{\ddagger}$ was estimated to be 67 kJ mol^{-1}, which is slightly larger than that reported for **[Me-Im][FSI]** with n = 12 ($\Delta G^{\ddagger}$ = 64 kJ mol^{-1}). These results indicate that $\Delta G^{\ddagger}$, which governs the atropisomerisation ability, can be tuned by controlling the bulkiness of the substituent at the 2-position of the imidazolium rings. At a $\Delta G^{\ddagger}$ value of 67 kJ mol^{-1}, atropisomer interconversion occurs in solution, but this process may be suppressed in the bulk state.

In general, ionic compounds composed of polar/non-polar parts exhibit thermotropic LC behaviour in the bulk state.[4,5] A key driving force for self-organisation is nanosegregation

between the ionic and non-ionic aliphatic parts. **[Me-Im][X]** forms Col_h or gyroid-Cub_{bi} phases depending on the temperature.[8] The thermotropic LC behaviours of **[H-Im][X]** and **[Et-Im][X]** were examined using polarised optical microscopy, differential scanning calorimetry (DSC), and X-ray diffraction (XRD) measurements. The exhibition of gyroid-Cub_{bi} and Col_h phases was observed independent of the substituent at the 2-position of the imidazolium rings and the anion (Fig. 4a). For example, when cooled from an isotropic liquid state, **[H-Im][TFSI]** showed a focal conic texture at approximately 70 °C (Fig. 4b, left), which is characteristic of the Col_h phase. Upon further cooling, dark domains with no birefringence appeared at approximately 50 °C (Fig. 4b, centre). These non-birefringent domains grew as the temperature decreased until the birefringence of the Col_h phase completely disappeared (Fig. 4b, right). This change is attributed to a transition from the Col_h phase to the Cub_{bi} phase, which has a cubic periodic structure. The phase-transition temperatures were confirmed using DSC, and the formation of Col_h and Cub_{bi} phases was confirmed using XRD (see the ESI). The phase-transition temperatures and mesophase patterns of the other compounds were characterised in the same manner.

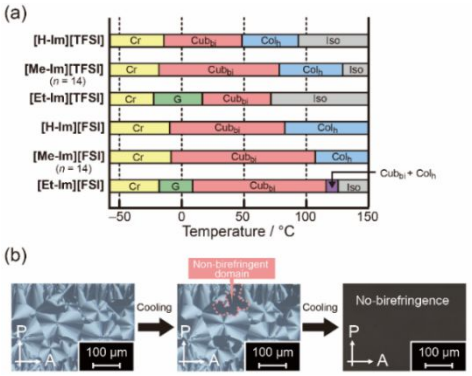

Fig. 4. (a) Thermotropic LC properties of **[H-Im][X]**, **[Me-Im][X]**,[8] and **[Et-Im][X]** upon cooling. Cr, crystalline; G, glassy; Col_h, hexagonal columnar; Cub_{bi}, bicontinuous cubic; Iso, isotropic. (b) Polarised optical microscopy images of **[H-Im][TFSI]** at the phase transition from the Col_h to Cub_{bi} phases.

To confirm the formation of Cub_{bi} LC assemblies, synchrotron XRD measurements were performed and 3D electron-density maps were reconstructed. This approach is a powerful strategy for revealing the molecular-assembly structures of fluidic LC materials.[11] The XRD pattern of **[H-Im][TFSI]** in the Cub_{bi} phase is shown in Fig. 5a. Two intense peaks corresponding to (211) and (220) reflections and some weak peaks are observed, which is characteristics of the formation of a gyroid-Cub_{bi} phase with $Ia\bar{3}d$ space group. By using the diffractogram, the most plausible 3D electron density map (ρ-map) has been constructed (Fig. 5b and the ESI) and the gyroid nanostructure formed by **[HIm][TFSI]** is successfully visualized. It can be seen that the gyroid-Cub_{bi} phase is composed of 3D continuous branched nanochannel domains with high electron density and a sheath domain with low electron density. These results clearly suggest that the ionic part of these molecules form a 3D continuous nanochannels while the non-ionic alkyl chain part form the surrounding domain. A similar XRD diffractogram was observed for **[Et-Im][TFSI]** (Fig. 5c), which produced a similar 3D ρ-map, albeit with some differences. To clarify these differences, we visualised the isoelectron surfaces showing the high-electron-density regions (highest 10%) of the two compounds (Fig. 5e and 5f). The junction areas in **[Et-Im][TFSI]** are more triangular, as clearly revealed by overlaying the two maps (Fig. 5g). Considering that gyroid-Cub_{bi} phases appear between columnar and smectic phases, the presence of triangular junctions indicates the formation of a gyroid-Cub_{bi} phase having a similarity to a layered smectic phase, whereas the presence of sharp junctions indicates the formation of a gyroid-Cub_{bi} phase having a similarity to a cylindrical columnar phase. Thus, we assume that the formation of sharp junctions in **[H-Im][TFSI]** is ascribed to a helical twisted molecular shape, while that of the flat triangular junctions in **[Et-Im][TFSI]** is ascribed to a less twisted molecular structure, even though there is no direct evidence for comparing the twistedness of these two compounds in bulk.

It should be noted that in **[Et-Im][TFSI]** a significant diffuse scattering hump is observed below the Bragg peaks (211) and (220) (Fig. 5c). This suggests a more significant amount of disorder in the sample, where local defects/distortions reduces the long range order. We speculate that such local defects/distortions may originate from imperfect local separation of atropisomers of opposite chiralities, but it remains to be investigated in the future.

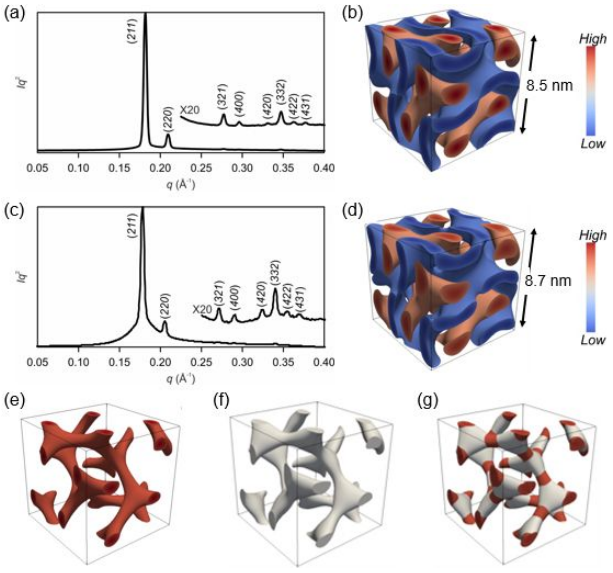

Fig. 5. (a) Powder XRD pattern of **[H-Im][TFSI]** in the gyroid-Cub_{bi} phase recorded at 45 °C during cooling. (b) 3D ρ-map of gyroid-Cub_{bi} in **[H-Im][TFSI]** at 45 °C. (c) Powder XRD pattern of **[Et-Im][TFSI]** in the gyroid-Cub_{bi} phase recorded at 60 °C during cooling. (d) 3D ρ-map of gyroid-Cub_{bi} in **[Et-Im][TFSI]** at 60 °C. (e,f) Isoelectron surfaces enclosing high-electron-density regions (highest 10%) in the unit cells of **[H-Im][TFSI]** (red) and **[Et-Im][TFSI]** (white), which appear as cylinder-like segments in the bicontinuous network. (g) Overlay of high-ρ regions in the gyroid-Cub_{bi} phases formed by the two compounds.

These ionic liquid crystals can potentially be applied as ion-conductive media.[5,12] Alternating-current impedance measurements revealed that **[Et-Im][TFSI]** has ionic conductivities of the order of 10^{-7} S cm^{-1} at 50 °C (see the ESI). These low values are attributed to the double-ionic structures of these compounds, which significantly increase the viscosity. The ionic liquid crystals also have potential as gas separation

and barrier materials[13] because of the superior ability of ionic liquids to absorb polar gases, especially CO_2.[14] Recently, the introduction of rigid structures such as spiro-centres into polymer main chains has been reported to increase the gas permeability of polymer membranes because the poor packing efficiency of these polymers produces a high free volume.[15] Considering these recent design strategies in polymer chemistry, we expect that the presence of sterically hindered structures in the present liquid crystals may facilitate the construction of nanopathways for CO_2 transportation. A first attempt towards polymerisable LC analogous of these V-shaped ionic liquid crystals with 1,3-diene groups is described in the ESI.

We successfully prepared a series of V-shaped ionic liquid crystals with sterically congested imidazolium groups. The occurrence of atropisomerisation in solution was strongly dependent on the bulkiness of the substituent at the 2-position of the imidazolium rings. The two imidazolium rings resulted in axial chirality, and the rotational barrier was 60–70 kJ mol^{-1} when a methyl or ethyl group was attached to the 2-position of the imidazolium rings. Based on this value, bond rotation is expected to be feasible in solution but suppressed in an aggregated state. Independent of the atropisomerisation ability in solution, the ionic liquid crystals formed gyroid-Cub_{bi} phases in the bulk state. For these compounds, we expect that gyroid-Cub_{bi} phase formation is partially promoted by atropisomerisation, with the main driving force being volume balance between the ionic and non-ionic parts. These results demonstrate that endowing LC molecules with the ability to form atropisomers has potential for the design of self-assemblies that form gyroid nanostructures.

T.I.: Conceptualisation, Supervision, Project administration, Funding acquisition, Writing – original draft. S.O. and S.Y.: Investigation, Data curation, Formal analysis. Y.T., T.K., and X.Z.: Investigation, Analysis.

This work was supported by the Japan Science and Technology Agency (JST) FOREST (JPMJFR223C) and JSPS KAKENHI (23K17937 and 24K01547) from the Japan Society for the Promotion of Science. We thank Drs Olga Shebanova and Nick Terrile at Station I22, Diamond Light Source, for help with SAXS experiment.

Data availability

The data supporting this article have been included as part of the ESI.†

Conflicts of interest

There are no conflicts to declare.

Notes and references

1 (a) M. Impéror-Clerc, *Curr. Opin. Colloid Interface Sci.,* 2005, **9**, 370; (b) D. W. Bruce, *Acc. Chem. Res.*, 2000, **33**, 831; (c) P. Fuchs, C. Tschierske, K. Raith, K. Das and S. Diele, *Angew. Chem., Int. Ed.,* 2002, **41**, 628; (d) X. Zeng, G. Ungar and M. Impéror-Clerc, *Nat. Mater.,* 2005, **4**, 562; (e) S. Kutsumizu, *Isr. J. Chem.*, 2012, **52**, 844.

2 (a) C. Fong, T. Le and C. J. Drummond, *Chem. Soc. Rev.*, 2012, **41**, 1297; (b) Y. Saadat, O. Q. Imran, C. O. Osuji and R. Foudazi, *J. Mater. Chem. A*, 2021, **9**, 21607; (c) G. P. Sorenson, K. L. Coppage and M. K. Mahanthappa, *J. Am. Chem. Soc.,* 2011, **133**, 14928; (d) B. R. Wiesenauer and D. L. Gin, *Polym. J.*, 2012, **44**, 461.

3 S. Diele, *Curr. Opin. Colloid Interface Sci.*, 2002, **7**, 333.

4 (a) K. Goossens, K. Lava, C. W. Bielawski and K. Binnemans, *Chem. Rev.,* 2016, **116**, 4643; (b) K. V. Axenov and S. Laschat, *Materials,* 2011, **4**, 206; (c) K. Binnemans, *Chem. Rev.,* 2005, **105**, 4148; (d) N. Kapernaum, A. Lange, M. Ebert, M. A. Grunwald, C. Haege, S. Marino, A. Zens, A. Taubert, F. Giesselmann and S. Laschat, *ChemPlusChem*, 2022, **87**, e20210039.

5 (a) T. Kato, M. Yoshio, T. Ichikawa, B. Soberats, H. Ohno and M. Funahashi, *Nat. Rev. Mater.*, 2017, **2**, 17001; (b) B.-K. Cho, A. Jain, S. M. Gruner and U. Wiesner, *Science,* 2004, **305**, 1598; (c) T. Ichikawa, M. Yoshio, A. Hamasaki, T. Mukai, H. Ohno and T. Kato, *J. Am. Chem. Soc.,* 2007, **129**, 10662; (d) T. Ichikawa, M. Yoshio, A. Hamasaki, J. Kagimoto, H. Ohno and T. Kato, *J. Am. Chem. Soc.*, 2011, **133**, 2163; (e) T. Ichikawa, T. Kato and H. Ohno, *J. Am. Chem. Soc.,* 2012, **134**, 11354.

6 (a) X. Lu, V. Nguyen, M. Zhou, X. Zeng, J. Jin, B. J. Elliott and D. L. Gin, *Adv. Mater.,* 2006, **18**, 3294; (b) M. Zhou, P. R. Nemade, X. Lu, X. Zeng, E. S. Hatakeyama, R. D. Noble and D. L. Gin, *J. Am. Chem. Soc.*, 2007, **129**, 9574; (c) M. Henmi, K. Nakatsuji, T. Ichikawa, H. Tomioka, T. Sakamoto, M. Yoshio and T. Kato, *Adv. Mater.,* 2012, **24**, 2238; (d) T. Sakamoto, T. Ogawa, H. Nada, K. Nakatsuji, M. Mitani, B. Soberats, K. Kawata, M. Yoshio, H. Tomioka, T. Sasaki, M. Kimura, M. Henmi and T. Kato, *Adv. Sci.,* 2018, **5**, 1700405.

7 (a) C. Dressel, T. Reppe, M. Prehm, M. Brautzsch and C. Tschierske, *Nat. Chem.*, 2014, **6**, 971; (b) C. Dressel, F. Liu, M. Prehm, X. Zeng, G. Ungar and C. Tschierske, *Angew. Chem., Int. Ed.*, 2014, **53**, 13115; (c) T. Yamamoto, I. Nishiyama, M. Yoneya, and H. Yokoyama, *J. Phys. Chem. B*, 2009, **113**, 11564.

8 N. Uemura, T. Kobayashi, S. Yoshida, Y. Li, K. Goossens, X. Zeng, G. Watanabe and T. Ichikawa, *Angew. Chem., Int. Ed.*, 2020, **59**, 8445.

9 (a) C. Escolásticor, M. D. S. María, R. M. Claramunt, M. L. Jimeno, I. Alkorta, C. Foces-Foces, F. H. Félix Hernández Cano and J. Elguero, *Tetrahedron*, 1994, **50**, 12489; (b) R. M. Claramunt, C. Escolástico and J. Elguero, *ARKIVOC*, 2001, **1**, 172.

10 K. R. Gibson, L. Hitzel, R. J. Mortishire-Smith, U. Gerhard, R. A. Jelley, A. J. Reeve, M. Rowley, A. Nadin and A. P. Owens, *J. Org. Chem.*, 2002, **67**, 9354.

11 (a) D. R. Dukeson, G. Ungar, V. S. K. Balagurusamy, V. Percec, G. A. Johansson and M. Glodde, *J. Am. Chem. Soc.*, 2003, **125**, 15974; (b) T. Ichikawa, M. Yoshio, A. Hamasaki, S. Taguchi, F. Liu, X. Zeng, G. Ungar, H. Ohno and T. Kato, *J. Am. Chem. Soc.*, 2012, **134**, 2634; (c) X. Zeng, S. Poppe, A. Lehmann, M. Prehm, C. Chen, F. Liu, H. Lu, G. Ungar and C. Tschierske, *Angew. Chem., Int. Ed.*, 2019, **58**, 7375; (d) T. Kobayashi, Y. Li, A. Ono, X. Zeng and T. Ichikawa, *Chem. Sci.*, 2019, **10**, 6245.

12 M. Yoshio, T. Mukai, H. Ohno and T. Kato, *J. Am. Chem. Soc.*, 2004, **126**, 994.

13 X. Lu, V. Nguyen, M. Zhou, X. Zeng, J. Jin, B. J. Elliott and D. L. Gin, *Adv. Mater.*, 2006, **18**, 3294.

14 (a) M. B. Shiflett and A. Yokozeki, *Ind. Eng. Chem. Res*., 2010, **49**, 1370; (b) Z. Lei, C. Dai and B. Chen, *Chem. Rev.*, 2014, **114**, 1289; (c) G. Gurau, H. Rodrguez, S. P. Kelley, P. Janiczek, R. S. Kalb and R. D. Rogers, *Angew. Chem., Int. Ed.*, 2011, **50**, 12024; (d) E. D. Bates, R. D. Mayton, I. Ntai and J. H. Davis Jr., *J. Am. Chem. Soc.*, 2002, **124**, 926; (e) R. E. Baltus, B. H. Culbertson, S. Dai, H. Luo and D. W. DePaoli, *J. Phys. Chem. B*, 2004, **108**, 721.

15 (a) P. M. Budd, B. S. Ghanem, S. Makhseed, N. B. McKeown, K. J. Msayib and C. E. Tattershall, *Chem. Commun.*, 2004, 230; (b) C. G. Bezzu, M. Carta, A. Tonkins, J. C. Jansen, P. Bernardo, F. Bazzarelli and N. B. McKeown, *Adv. Mater.*, 2012, **24**, 5930.

Data availability statement

The data supporting this article have been included as part of the Supplementary Information.